JJBS

Volume 15, Number 3,September 2022
ISSN 1995-6673
Pages 511 – 522
https://doi.org/10.54319/jjbs/150321

Jordan Journal of Biological Sciences

Response Surface Method for Optimizing the Biosynthesis of Silver Nanoparticles Using *Talaromyces stipitatus* and Their Antimicrobial Activity

Nada M. Elmayah*, Amira A. El-Fallal, Mohamed I. Abou-Dobara, Mahmoud E. Khalifa

Department of Botany and Microbiology, Faculty of Science, Damietta University, New Damietta, Egypt.

Received: May 29, 2021; Revised: August 16, 2021; Accepted: October 4, 2021

Abstract

Central composite design (CCD) as one of response surface designs was employed to optimize the biosynthesis process of silver nanoparticles (AgNPs). In this design, fungal cell-free filtrate of *Talaromyces stipitatus* was applied as a biosource for the biosynthesis of AgNPs. Different variables with five levels were used to optimize AgNPs biosynthesis. Independent variables were concentration of silver nitrate ($AgNO_3$; mmole), temperature (°C), time, pH and ratio of $AgNO_3$ to cell free extract. While dependent variable was peak intensity of surface plasmon resonance (SPR) at wavelength 420 nm. The predicted optimal setup parameters were $AgNO_3$ concentration of 7 mmol, temperature of 25 °C, time of 91.2 hr, pH of 8 and ratio of $AgNO_3$ solution to cell-free extract of 2:1. The characteristics of biosynthesized AgNPs were revealed using Fourier transform infrared spectroscopy (FTIR), dynamic light scattering (DLS), zeta potential, energy dispersive x-ray analysis (EDX), and transmission electron microscopy (TEM). Biosynthesized AgNPs appeared to be spherical, with mean size of 13.95 nm and zeta potential of 9.85 mV. Biosynthesized AgNPs were also examined for their antimicrobial properties against selected bacterial and fungal pathogens including *Staphylococcus aureus*, *Bacillus cereus*, *Pseudomonas aeruginosa*, *Klebsiella pneumoniae*, *Aspergillus flavus*, *A. niger*, *Fusarium oxysporum* and *Alternaria alternata*.

Keywords*:* Nanoparticles, silver, *Talaromyces stipitatus*, antibacterial, antifungal,

1. Introduction

Nanotechnology is identified as the control or transformation of a substance at the nano scale, normally at sizes extending from 1 to 100 nm. Nanomaterials and nanoparticles (NPs) are considered the fundamental components of nanotechnology (Phanjom & Ahmed, 2017). Owing to the fact that the features of transformed substances (at the nano scale) vary greatly from those of their macro scale original forms. NPs have peculiar physicochemical properties, i.e., high reactivity, larger surface area and unique particle morphology (Siddiqui et al., 2015). In the early stage of substance transformation into the nano scale, the properties remain almost unchanged. Afterwards, minor variations arise until eventually drastic shifts in properties are noted when dimensions decrease to the nano scale, below 100 nm (Bhushan, 2017). The term "nano" is a prefix for one billionth (10^{-9}) and has its origin from the Latin word "nanos", meaning tiny.

Nanomaterials are generally obtained through two approaches; bottom-up and top-down. In the bottom-up approach, the process begins with a bulk material that gets split into smaller particles via chemical, mechanical or other (top-down) energy forms. The second approach (bottom-up) is to synthesize the substance by chemical reactions from atomic or molecular precursors that gradually grow in size (Ahumada et al., 2019). Metal NPs are of significant scientific importance in bridging the gap between the bulk structures and atomic structures. Silver nanoparticles (AgNPs), a remarkable type of metallic NPs, have become more widespread and are currently used in several fields, including food storage and industry, in addition to medicine as they have effective antimicrobial activities (Vega-Baudrit et al., 2019).

AgNPs biosynthesis is a bottom-up strategy that depends mainly on reduction and oxidation reactions (Majeed et al., 2019; El-Zahed et al., 2021). For the synthesis of AgNPs, several preparation strategies with diverse processes have been proposed including chemical, physical, and biological approaches (Ahumada et al., 2019; Baker et al., 2015). Green nanotechnology has risen in popularity on account of the current surge in the creation of environmentally friendly technologies, leading to an evolution of diverse studies on natural reducing agents utilized in NPs synthesis (Bhatnagar et al., 2019). The biological approach or green synthesis system, called nanobiotechnology, is usually classified as a modern nanotechnology (Basavegowda & Lee, 2014).

In the production of AgNPs, bio-extracts from microorganisms can function as reducing and/or capping agents. Combinations of biomolecules included in these extracts, such as enzymes, amino acids, vitamins,

* Corresponding author. e-mail: Nada_elmayah.20@yahoo.com.

polysaccharides and proteins, can help in reducing Ag^+ ions (Collera-Zúñiga et al., 2005; Jagadeesh et al., 2004; Kate et al., 2020).

Given the drawbacks of utilizing classical experimental optimization methods, by employing statistical experimental design and response surface method (RSM) to optimize all of the influencing factors, the drawbacks of a single factor optimization procedure may be eliminated (Baş & Boyacı, 2007). RSM has been commonly used to achieve the optimal conditions required for several biotechnological processes by assessing the interaction impact of model variables (Guo et al., 2016).

In the present study, a fungal cell-free extract was applied to biosynthesis of ecofriendly and low-cost AgNPs. The effect of different factors influencing AgNPs production was optimized using central composite design (CCD) as one of RSM. This method provided us little number of trial-and-error runs is usually performed. Reports on using this experimental design and also *Talaromyces stipitatus* fungus in green synthesis of AgNPs are rare.

2. Materials and methods

2.1. Chemicals

Different culture media for routine culturing of fungal and bacterial strains were purchased from Difco Laboratories (Detroit, Mich., USA); silver nitrate ($AgNO_3$) was provided by Panreac Quimica (S.L.U, Barcelona, Spain); and HNO_3 (0.1 M), NaOH (0.1 M) solution used in pH measurements and all other chemicals were purchased from Oxoid Ltd. (Hampshire, UK).

2.2. Instruments

Several instruments used in this study included Ultraviolet Spectrum (origin: JASCO, model: V-630); Infrared Spectrum (origin: JASCO, model: FT/IR-4100 type A), Zeta Potential Analyzer (origin: Malvern Instruments Ltd, model: Malvern Zetasizer Nano-zs90), Transmission Electron Microscope (TEM) (model: JEOL JEM-2100); Energy-dispersive X-ray spectroscopy (EDS) (Oxford instrument, model: Oxford X-Max 20), and a pH meter.

2.3. The fungal strain used for biosynthesis of AgNPs

The fungal strain used in this research was previously isolated from Lake Burullus, Egypt and identified as *Talaromyces stipitatus* by Botany and Microbiology Department, Faculty of Science, Damietta University, using classical morphological methods and confirmed by sequencing the internal transcribed spacer (ITS) region using universal primers ITS4 and ITS5 (White et al., 1990).

2.4. Preparation of fungal extract

Cell-free fungal filtrate of *T. stipitatus* was prepared to be applied in the biosynthesis of AgNPs. Firstly, to obtain fungal biomass, 250 ml Erlenmeyer flasks containing 100 ml of nitrate medium (0.35% yeast extract, 1% peptone, 0.35% potassium nitrate, and 1.5% glucose) (Hamedi et al., 2017) were inoculated with 5-day old discs of *T. stipitatus* and grown at 30°C for 7 day. For extracellular biosynthesis of AgNPs, wet fungal biomass was shaken for 72 h in 100 ml of sterilized distilled water at 150 rpm and 30° C. The cell-free filtrate was collected by filtration through Whatman filter paper no. 1.

2.5. Designing experiments for optimizing AgNPs production Talaromyces stipitatus

To prepare AgNPs, cell-free filtrate and $AgNO_3$ solution (1mM) were mixed and incubated at 30°C with agitation (150 rpm) for 120 hours in the dark. Initially, development of brown color is considered as an indication for the biosynthesis of AgNPs. A set of experiments were designed based on CCD changing the independent variables (temperature, reaction time, concentration of $AgNO_3$, and ratio of cell free extract and $AgNO_3$) considering absorbance at wavelength 420 nm as response (Table 1). Design was built with a total of 32 runs, and SPR intensity was recorded for each run.

Table 1. The different variables and their levels used for optimization of AgNPs biosynthesis by *Talaromyces stipitatus*.

	Independent variable (actual value)				
	A	B	C	D	E
Level (coded value)	concentration of $AgNO_3$ (mmol)	Temperature (C°)	Time of reaction (day)	pH	ratio of $AgNO_3$ solution to cell free extract
-2 (−α)	1	20	1	5	3:1
-1	3	25	2	6	2:1
0	5	30	3	7	1:1
1	7	35	4	8	1:2
2(+α)	9	40	5	9	1:3

In 32 CCD-designed runs, there were 16 factorial runs included as cubic points, and 6 center points as replication runs used for pure error clarification. In addition, 8 axial runs were incorporated as star points of the proposed CCD. The alpha star points were set to a value of 2, so as to provide a rotatable design for experiments. The response was represented and indicated as “Peak intensity” of the SPR which obtained by measuring the absorbance of 32 produced AgNPs samples at 420 nm.

The analysis of results and the building of experimental design were created using graphical and statistical analysis software (Design Expert ®, Version 11.0.0) and all experiments were carried out in triplicates. The first step in performing the statistical analysis using a multivariate optimization was to construct a regression model between

the intensity of the SPR (target response) and the experimental factors as the model's independent variables.

Different linear and polynomial regression models and various statistical parameters such as Sequential p-value, Lack of Fit p-value and squared correlation coefficient (R^2) as "Adjusted R^2" and "Predicted R^2" were tested to select the best regression model.

The following second order polynomial equation was applied to calculate the relationship between different variables and the response:

$$Y = ß_0 + \sum ß_i X_i + \sum ß_{ii} X_i^2 + \sum ß_{ij} X_i X_j \quad \text{(eq.1)}$$

where Y is the expected response, Xi, Xi^2, and Xj are variables with coded values, ß0 is the constant, ßi is the linear effect, ßii is the squared effect, and ßij is the interaction effect.

2.6. Characterization of AgNPs

Nanoparticle size, morphology and shape were studied using TEM (Zhang et al., 2016). The particle size and zeta potential in liquid suspension were measured at 25°C using a Zeta Potential Analyzer. Energy-dispersive X-ray spectroscopy (EDX) was used as a standard approach for defining and quantifying elemental composition of samples. To estimate the functional components of synthesized AgNPs, Fourier transform infrared (FTIR) spectrum was analyzed.

2.7. Antibacterial activity

Potential antibacterial activity of biosynthesized AgNPs against Gram-positive bacteria such as *Staphylococcus aureus* ATCC25923 and *Bacillus cereus* ATCC6633, and Gram-negative bacteria like *Pseudomonas aeruginosa* ATCC27853 and *Klebsiella pneumoniae* ATCC33495 was firstly checked using the disk diffusion method.

First, 0.5 McFarland ($1.5*10^8$ CFU/mL) of overnight pathogenic bacterial cultures were prepared. The bacterial growth was then inoculated into molten Mueller Hinton (MH) agar, resulting in a final concentration of tested strains of approximately 10^6 cfu/ml. After solidification, 15 mm-diameter pores were made on agar plates and 200 µL of AgNPs (50, 100, 200 µg/ml) were added in each pore. Also, solutions of $AgNO_3$ (1 mmole), fungal cell-free filtrate of *T. stipitatus* and standard commercial antibiotic disks were used as controls. Following an incubation period of 24 h at 37° C, diameters of inhibition zone were assessed in millimeters (mm). The tests were all performed in triplicate.

Using a broth microdilution methodology, the biosynthesized NPs were experimented for their minimum inhibitory concentrations (MIC) against pathogenic bacteria. AgNPs (64 g/ml) solution was serially diluted by Mueller-Hinton (MH) broth to get concentrations (32, 16, 8, 4, 2, 1, 0.5, 0.25 g/ml). In this experiment, bacterial inocula (final concentration of 10^6 CFU/ml) were placed in wells of a microtiter plate and different controls were included, i.e., culture media, cultures inoculated with tested strains, and culture media supplemented with AgNPs solely without inocula. The microtiter plate was kept at 37 °C for 24h, then the bacterial turbidity was measured spectrophotometrically and growth confirmed by re-culturing on MH agar plates. MIC values were determined by taking the lowest concentration leading to no growth on plates. The trials were carried out in two repetitions.

2.8. Antifungal activity

Antifungal activity of AgNPs against *Aspergillus flavus* Link ex Fries group, *Aspergillus niger* van Tiegh, *Fusarium oxysporum f. sp. lycopersici* Fol4287 and *Alternaria alternata* Fr. Keissler was carried out on PDA media. Tested fungal strains were obtained from Botany and Microbiology Department, Faculty of Science, Damietta University.

PDA plates supplemented with different AgNPs concentrations (1, 2, 4, 8, 16, 32 and 64 mg/l), with fluconazole (0.01 g/ml) as an antifungal agent (positive control) and without any treatment (negative control) were used. Each treatment was replicated. Disks (6 mm in diameter) of 7-day old fungal were placed upside-down in the center of the plates, incubated for 5 days and the radial growth was measured.

3. Results and discussion

3.1. Optimization of AgNPs production using response surface methodology

Table 2 shows 32 CCD-designed runs with the results of response as SPR intensity.

Table 2. Details of the 32 runs performed using central composite design (CDD) to optimize the biosynthesis of AgNPs.

Run	A Concentration of $AgNO_3$ (mmole)	B Temperature (°C)	C Time (day)	D pH	E ratio of gNO_3 to cell free extract	Absorbance Intensity*
1	-1	1	1	-1	1	0.204831
2	-1	1	-1	-1	-1	0.361102
3	-1	1	1	1	-1	0.432689
4	0	0	0	0	0	0.418252
5	-1	-1	1	1	1	0.214648
6	1	-1	-1	1	1	0.229373
7	0	2	0	0	0	0.480851
8	1	1	1	-1	-1	0.713129
9	0	0	0	0	2	0.426267
10	1	1	-1	1	-1	0.543788
11	0	0	0	2	0	0.874823
12	0	-2	0	0	0	0.429624
13	0	0	0	0	0	0.474823
14	-2	0	0	0	0	0.261278
15	1	-1	1	1	-1	0.747416
16	0	0	2	0	0	0.134135
17	-1	-1	-1	1	-1	0.418703
18	0	0	0	0	0	0.408007
19	0	0	-2	0	0	0.267079
20	0	0	0	0	0	0.408007
21	0	0	0	0	0	0.200634
22	1	1	-1	-1	1	0.388326
23	0	0	0	0	0	0.409437
24	0	0	0	-2	0	0.866519
25	1	1	1	1	1	0.318729
26	1	-1	-1	-1	-1	0.433972
27	1	-1	1	-1	1	0.535898
28	-1	1	-1	1	1	0.353926
29	2	0	0	0	0	0.701836
30	-1	-1	-1	-1	1	0.260633
31	-1	-1	1	-1	-1	0.196726
32	0	0	0	0	-2	0.411167

* The absorbance intensity of the SPR at 420 nm.

A quadratic model was proposed on the basis of these statistics to establish a correlation between the experimental variables and the response, as indicated in table 3. In this case, quadratic model was the highest order polynomial selection where the additional terms are significant and the model is not aliased; cannot be accurately fit with the design and should generally not be considered for analysis.

Table 3. Fit statistics of the quadratic model.

Std. Dev.	**0.1209**	**R^2**	**0.8555**
Mean	0.4227	Adjusted R^2	0.5927
C.V. %	28.60	Predicted R^2	-1.6546
		Adeq Precision	7.0880

: R^2 = Correlation Coefficient

Adequate precision (Adeq. Precision) seems to be another statistical indicator for our model validation and can be a measure of the ratio of signal to noise. In our model, ratio of 7.088 indicates an adequate signal (greater than 4), as the precision acceptance cut-off value. This model can be utilized to navigate the design space.

The computed parameters for the quadratic full model (FM), which included all experimental variables, were

$AgNO_3$ concentration (A), temperature (B), time of reaction (C), pH (D) and proportion of $AgNO_3$ to cell free extract (E) and their binary and self-interactions. The final equation with reference to coded factors was represented by the following equation in which SPR intensity of AgNPs (Y) was the response [eq (2)]:

SPR Intensity =0.407063 + 0.0978537 * A + 0.0159002 * B + 0.00451479 * C + 0.00755262 * D + -0.0546234 * E - 0.0152828 * AB + 0.0665739 * AC + -0.0392933 * AD + -0.0369248 * AE + -0.0206107 * BC -0.0125729 * BD + -0.0142894 * BE + -0.00242869 * CD + -0.0181592 * CE + -0.0444174 * DE + 0.00322165 * A^2 + -0.00335823 * B^2 + -0.0670159 * C^2 + 0.1005 * D^2 + -0.0124884 * E^2 (eq.2)

This equation with regard to coded factors may be applied to predict response for different levels of each factor and determine the relative importance of the components by contrasting the factor coefficients. For each factor, when all other factors are maintained constant, the coefficient estimate provides the predicted change in response per unit change in factor value. Based on Eq. 2, the sign of coefficient is negative for the ratio of $AgNO_3$ to cell free extract (factor E) and positive for the other four variables ($AgNO_3$ concentration, temperature, reaction time, and pH). This indicates that the ratio of $AgNO_3$ to cell free extract (factor E) reversely affect AgNPs biosynthesis, whereas $AgNO_3$ concentration (factor A), temperature (factor B), reaction time (factor C), and pH (factor D) have direct effect on AgNPs formation. Temperature effect of SPR intensity could be due to improving the formation rate of AgNPs. Increasing pH beneficially influence the intensity of SPR probably as a result of increasing the ionisation of active functional groups, the reduction capability of the extract and subsequently the formation of AgNPs. Raising $AgNO_3$ concentration results in improving AgNPs formation as indicated by darkening in solution and increased SPR peak intensity. Also, increasing reaction time increased AgNPs formation.

On the contrary, increasing $AgNO_3$ concentration while decreasing the volume of cell free extract resulted in an increasing in the AgNPs SPR intensity. Several studies indicated that for better AgNPs formation, excess silver ion is required in the biological /green synthesis approach (Dada et al., 2018). The SPR intensity decreased in a high volume of fungal cell-free extracts because of the high amounts of the reducing agents, that could promote AgNPs precipitation (Yakovlev & Golubeva, 2014).

As seen in Eq. (2), the positive sign of $AgNO_3$ concentration*time implied a direct influence of their interaction on AgNPs formation and quality as indicated by SPR intensity, whereas the negative sign of the other interaction reflects their reverse influence on AgNPs biosynthesis. The analysis of variance (ANOVA) was performed and results are presented in Table 4.

Table 4. ANOVA and model performance of full quadratic model.

Source	Sum of Squares	Df	Mean Square	F-value	p-value	
Model	0.9518	20	0.0476	3.26	0.0242	Significant
A- $AgNO_3$ conc.	0.2298	1	0.2298	15.72	0.0022	
B- temperature	0.0061	1	0.0061	0.4151	0.5326	
C- time	0.0005	1	0.0005	0.0335	0.8582	
D- pH	0.0014	1	0.0014	0.0937	0.7653	
E- ratio	0.0716	1	0.0716	4.90	0.0489	
AB	0.0037	1	0.0037	0.2557	0.6231	
AC	0.0709	1	0.0709	4.85	0.0499	
AD	0.0247	1	0.0247	1.69	0.2202	
AE	0.0218	1	0.0218	1.49	0.2474	
BC	0.0068	1	0.0068	0.4650	0.5094	
BD	0.0025	1	0.0025	0.1730	0.6854	
BE	0.0033	1	0.0033	0.2235	0.6456	
CD	0.0001	1	0.0001	0.0065	0.9374	
CE	0.0053	1	0.0053	0.3610	0.5602	
DE	0.0316	1	0.0316	2.16	0.1697	
A^2	0.0003	1	0.0003	0.0208	0.8879	
B^2	0.0003	1	0.0003	0.0226	0.8831	
C^2	0.1317	1	0.1317	9.01	0.0120	
D^2	0.2963	1	0.2963	20.27	0.0009	
E^2	0.0046	1	0.0046	0.3130	0.5871	
Residual	0.1608	11	0.0146			
Lack of Fit	0.1160	6	0.0193	2.16	0.2082	not significant
Pure Error	0.0448	5	0.0090			
Cor Total	1.11	31				

DF = Degree of Freedmen, F = Fisher-ratio.

Model terms are considered significant when the P-value is less than 0.0500 whereas values larger than 0.1000 imply that they are not significant. A, E, AC, C^2, and D^2 are significant model terms in this situation.. In addition,

the normal residual probability and the internally studied residual vs. the expected response (SPR intensity) are two more ways that may be used to assess the validity of the models. According to Figure 1 (a), for all the outstanding values reflected along the straight line with small value of deviations and proves the normality of errors-distribution. Figure 1(b) presents the relation of residual vs. predicted SPR intensity, the residual is randomly distributed in both sides of zero line and also lie in a range that is less than the allowable range of ±3σ.

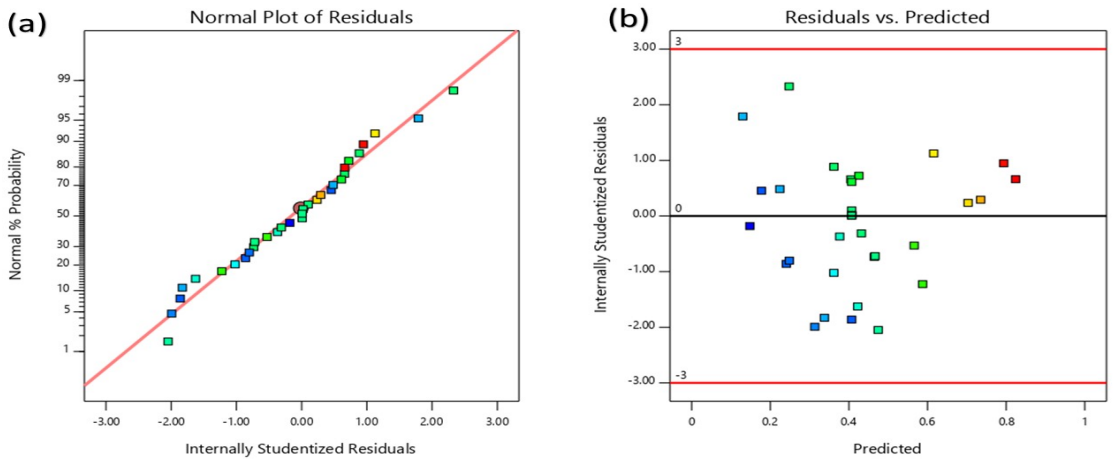

Figure 1. Normal probability plot of internally studentized residuals for the quadratic model for SPR intensity (**a**) and plot of residual versus predicted SPR intensity (**b**).

Using the three-dimensional (3D) response surface plots, the effect of different tested factors (independent variables) on the AgNPs SPR intensity (dependent variable) was studied (Figure 2). The graphs show SPR intensity as response surface, versus two factors that may show binary interactions. The other factors were set constant at the central level. Figure 2 (a) demonstrates that $AgNO_3$ concentration (A) has a greater influence on SPR intensity than time (C), since the surface slope is steeper in the direction of $AgNO_3$ concentration axis than towards time axis. Furthermore, temperature (B) has a greater influence on SPR intensity than ratio (E) (e). The surface slope obtained for temperature × $AgNO_3$ concentration was less steep than that obtained for time × concentration of $AgNO_3$ (Figure 2 (a, b)). AgNPs formation was improved at alkaline pH, as predicted and shown in Figure 2 (c). As shown in Figure 2 (d), $AgNO_3$ concentration (A) versus the ratio (E) was the steepest slope of the surface plots confirming that using amounts of $AgNO_3$ larger than the amount of cell-free filtrate improves the biosynthesis of AgNPs. It can be viewed in Figure 2 (f) that the interaction of time × pH is more complex since more curvature in the 3D plot surface was noted. Finally, because all of the produced surfaces are smooth in each plot and both factors have a comparable influence on the SPR intensity, there is no abnormal interaction between variables. Data obtained by the 3D response surface plots are in accordance with those obtained from quadratic model equation.

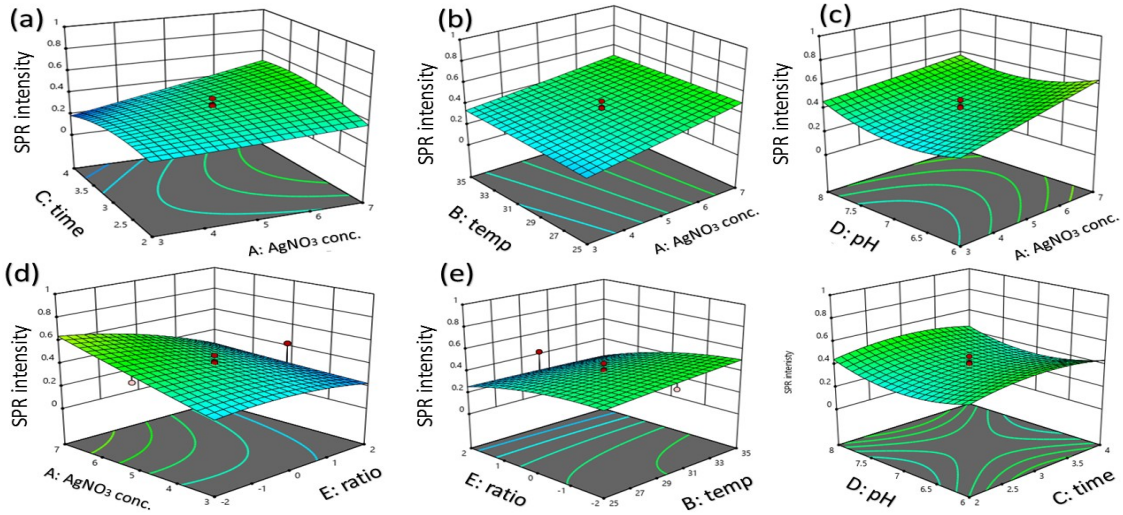

Figure 2. Three-dimensional response surface plots of independent factors effect [time–$AgNO_3$ concentration(**a**)], [temperature–$AgNO_3$ concentration (**b**)], [$AgNO_3$ concentration –pH (**c**)], [$AgNO_3$ concentration –ratio (**d**)], [ratio–temperature (e)], and [pH–time (**f**)] on the SPR intensity of AgNPs Optimal condition of AgNPs biosynthesis by T. stipitatus

To get maximum SPR intensity and thus obtaining high amounts of AgNPs, the predicted optimal conditions were determined to be: $AgNO_3$ concentration= 7mmol, temperature = 25°C, time= 91.2 hr, pH=8, ratio of $AgNO_3$ solution to cell free extract is 2:1. Some synthesized samples of AgNPs were prepared under these optimal conditions to verify the accuracy of this prediction as shown in Figure 3.

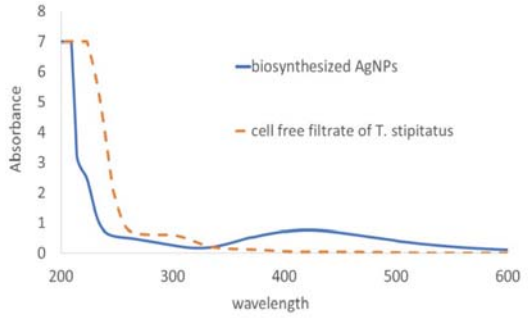

Figure 3. UV-Vis absorption spectra, showing the SPR peak, of synthesized AgNPs using cell free extract of *T. stipitatus*.

3.2. Characterization of synthesized silver nanoparticles

As shown in Figure 4, the biosynthesized AgNPs varied in size from 6.89 nm 23.64 nm and had spherical shapes. The average size of AgNPs based on different taken images is 13.95 nm. The size of AgNPs observed in TEM images is comparable with that obtained in previous studies focusing on AgNPs biosynthesis (Sharma et al., 2018); especially by fungi belonging to the same family of *Talaromyces* (Rose et al., 2019).

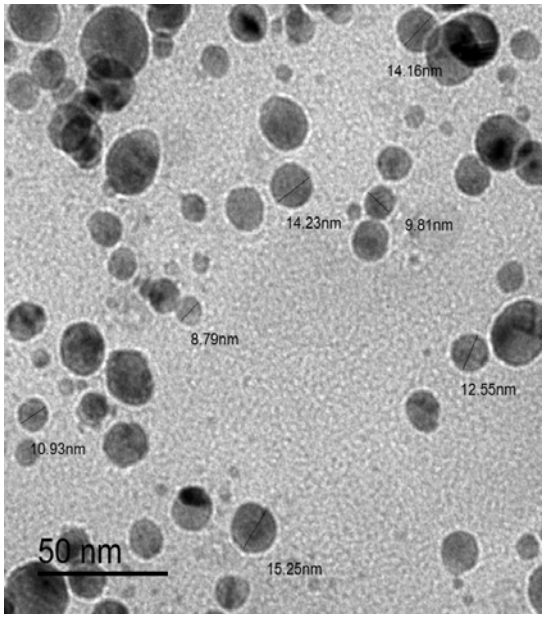

Figure 4. Transmission electron microscopy (TEM) micrograph of spherical AgNPs, biosynthesized by *Talaromyces stipitatus*.

In EDX analysis, the energy dispersive spectrum indicated the existence of elemental silver (Figure 5). As previously reported, at 3 keV, the sharp peak marked the presence of metallic silver (Femi-Adepoju et al., 2019). Also, the appearance of other EDX peaks for C, O, Na, k and Mo is probably due to the content of used cell-free filtrate.

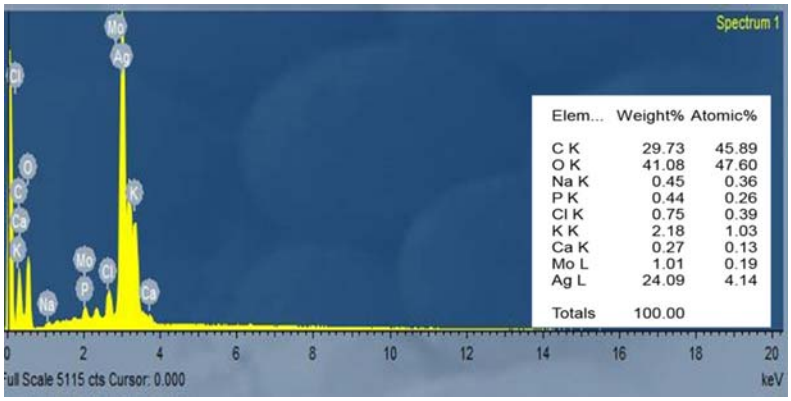

Figure 5. EDX spectrum of AgNPs biosynthesized by *Talaromyces stipitatus* filtrate.

The zeta potential, a measure indicator of NPs stability, was indicated to be 9.85 mV (Figure 6 (a)). NPs having a zeta potential of 0 to 10 mV are considered to be near to neutral state (Asha & Narain, 2020). The zeta potential value might be attributed to biomolecules contained in the employed cell-free fungal filtrate capping (Raja et al., 2017).

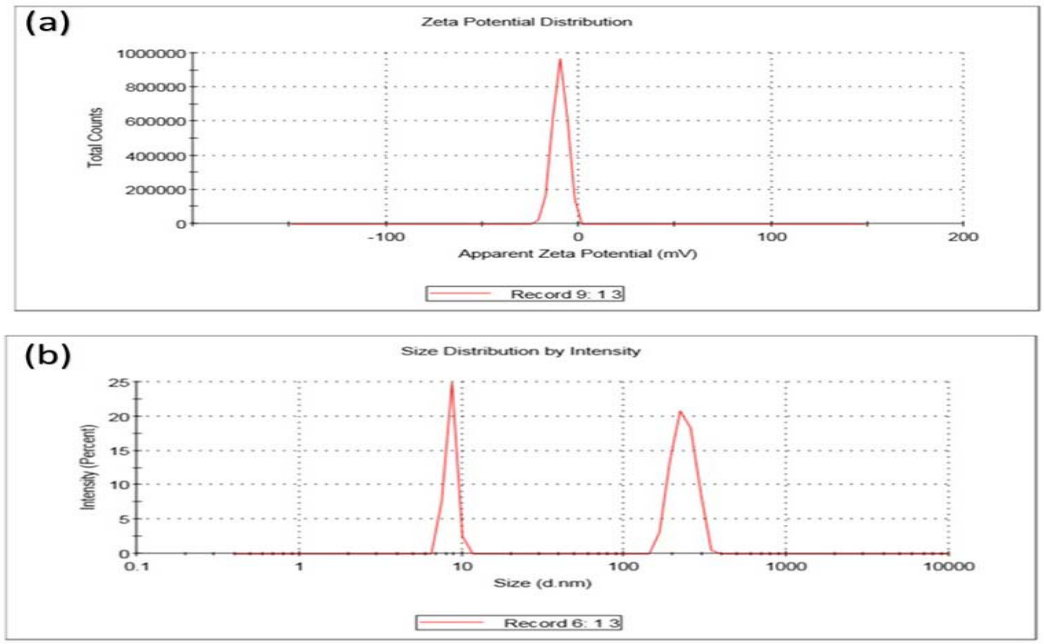

Figure 6: DLS and Zeta potential measurement using Zetasizer; **(a)**: Zeta potential and **(b)** Size Distribution chart, determined by intensity, using DLS for AgNPs sample biosynthesized by *Talaromyces stipitatus*

Using dynamic light scattering (DLS), the size distribution profile of AgNPs biosynthesized by *T. stipitatus* is presented in Figure 6 (b). The distribution curve shows two different peaks that represent different particle sizes with average size of 58.22 (d. nm). In fact, the size of 65% of particles was 232.1 d.mn, whereas that of remaining 35 % was 8.562 d. nm. It is considered that DLS measures the hydrodynamic radius, not the absolute radius. This measure depends on the velocity of the Brownian motion which is transformed into particle size using the Stokes-Einstein relationship (Zhang et al., 2016).

FTIR analysis was performed to identify the compounds and functional groups responsible for the reduction of Ag^{+} ions and capping of NPs. In Figure 7, the FTIR spectrum of biosynthesized AgNPs showed several noticeable peaks at 3408.57, 2142.53, 1623.77, 1395.25, 1038.48 and 623.85 cm^{-1}. The existence of band peak at 3408.57 cm^{-1} might be due to the presence of N-H stretching. The presence of silver nanomaterials in the composition of biosynthesized AgNPs is demonstrated by a clear band at 1623 cm^{-1} (Owaid et al., 2018). Also, the C-O stretching mode is responsible for the vibrations at 1,395 and 2,142 cm^{-1} (El-Naggar et al., 2014). Moreover, the band at 1038 cm^{-1} correspond to the amine's C-N stretching vibrations. The existence of a proteinaceous capping agent that inhibits NPs from aggregating has been suggested as a possible explanation for the stability of AgNPs produced using cell-free filtrates (Saifuddin et al., 2009).

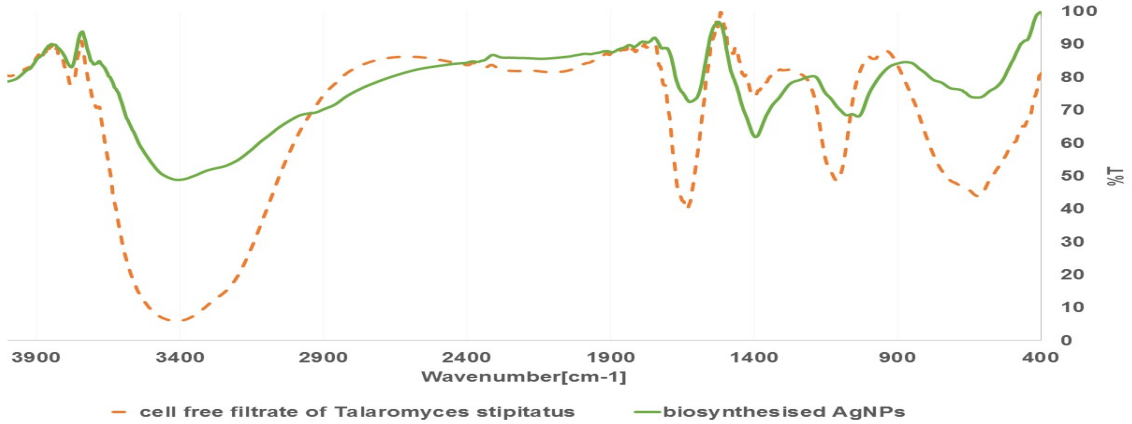

Figure7. FTIR spectrum of AgNPs biosynthesized by Talaromyces stipitatus

3.3. Antibacterial activity:

AgNPs synthesized by *T. stipitatus* were evaluated for their antibacterial activity by disk diffusion method and results were recorded in Table 5 and shown in Supplementary Figure 1. The MIC values were 4, 8, 16 and 8 µg/ml for *B. cereus*, *S. aureus*, *K. pneumoniae* and *P. aeruginosa*, respectively. The antibacterial activity results against *B. cereus* ATCC6633 was similar to that reported by Nour El-Dein et al., (2021).

Table 5. Inhibition effect of silver nanoparticles against selected pathogenic bacteria

Treatment	Diameter of inhibition (mm, mean)			
	Bacillus cereus ATCC6633	*Staphylococcus aureus* ATCC25923	*Klebsiella pneumoniae* ATCC33495	*Pseudomonas aeruginosa* ATCC27853
200 µg/ml AgNPs	19.11	16.1	19.15	18.36
100 µg/ml AgNPs	16.71	15.3	15.3	14.16
50 µg/ml AgNPs	12.63	12.86	12.84	11.43
Penicillin G	10.36	30.1	17.81	8.2
$AgNO_3$ (1 mmole)	10.06	12.01	15.1	12
cell free filtrate of *Talaromyces stipitatus*	-	-	-	-

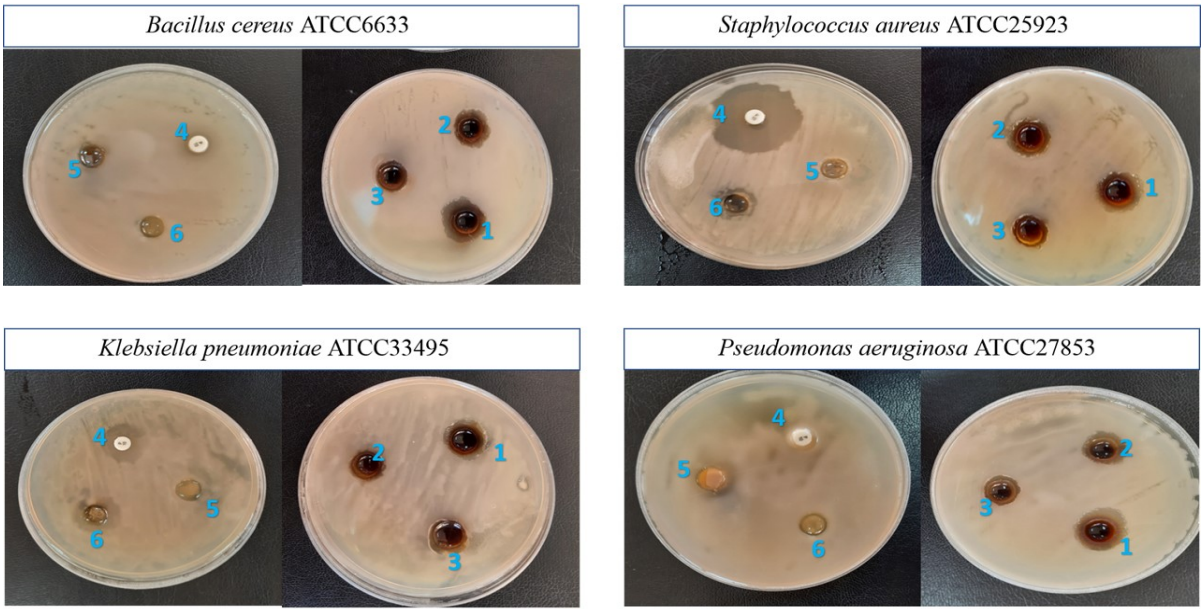

Figure 8. Inhibition zone of AgNPs against *B. cereus* ATCC6633, *S. aureus* ATCC25923, *P. aeruginosa* ATCC27853 and *K. pneumoniae* ATCC33495
note: (1) 200 µg/mL AgNPs, (2) 100 µg/mL AgNPs, (3) 50 µg/mL AgNPs, (4) Penicillin G, (5) $AgNO_3$ (1m. mole) and (6) cell free filtrate of *T. stipitatus* treatments

3.4. Antifungal activity:

The effect of different AgNPs concentrations on fungal growth was tested and data recorded and shown in Table 6 and Supplementary Figure 2. AgNPs synthesized by *T. stipitatus* appeared to be a promising control agent against *A. flavus* Link ex Fries group and *A. niger* van Tiegh as the growth diameter was reduced in rates comparable with the positive control, the antifungal compound fluconazole (0.01g/ml).

Table 6. Inhibition effect of silver nanoparticles against some fungi.

	Radial growth (mm) *			
Treatment	*Fusarium oxysporum f. sp. lycopersici* Fol4287	*Alternaria alternata* Fr. Keissler	*Aspergillus flavus* Link ex Fries group	*Aspergillus niger* van Tiegh
Negative control – without any treatment	64	64	82	85
Positive control -with antifungal compound-fluconazole (0.01g/ml)	54	24	71	79
1 mg/l of AgNPs	63	55	78	85
2 mg/l of AgNPs	62	52	77	82
4 mg/l of AgNPs	61	50	75	80
8 mg/l of AgNPs	60	47	73	78
16 mg/l of AgNPs	60	45.5	70	76
32 mg/l of AgNPs	59	45	65	72
64 mg/l of AgNPs	58	43	64	65

*mean

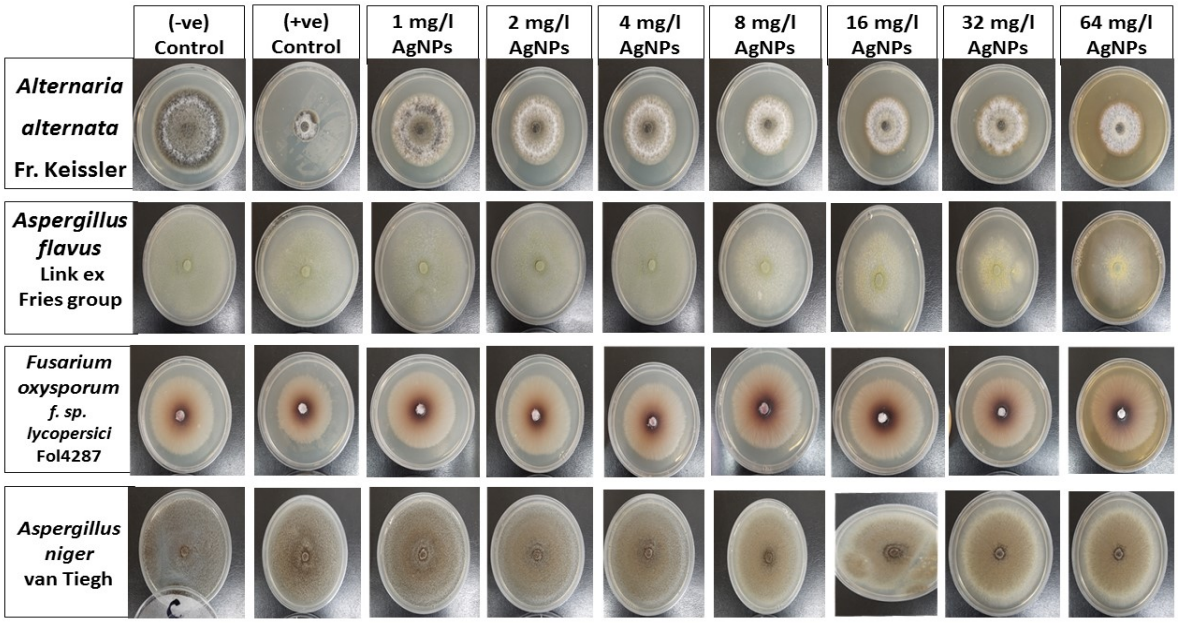

Figure 9. Visual radial growth for inhibitory effect of AgNPs against *Aspergillus* niger van Tiegh, *Aspergillus flavus* Link ex Fries group, *Alternaria alternata* Fr. Keissler and *Fusarium oxysporum* f. sp. lycopersici Fol4287.
note: AgNPs concentrations (1, 2, 4, 8, 16, 32 and 64 mg/L) and controls; Negative control: without any treatment and positive control: with antifungal compound-fluconazole (0.01g/ml).

4. Conclusion

T. stipitatus fungus was used as a green source for the biosynthesis of AgNPs. Fungal cell-free filtrate, including the metabolites, may work as reducing and capping reagent in the process of AgNPs biosynthesis. It helps stabilizing the produced AgNPs by converting Ag+ ions to Ag°. Different factors including temperature, pH, and time of reaction may affect this process. Therefore, in the current study, CCD was used for optimizing AgNPs biosynthesis process. Five factors were evaluated in the optimization process of NPs biosynthesis by fungal cell-free filtrate, i.e., concentration of $AgNO_3$ (mmole), temperature (°C), time, pH and ratio of $AgNO_3$ to cell free extract. Using CDD, the optimal conditions were predicted to be: $AgNO_3$ concentration= 7mmol, temperature = 25 °C, time= 91.2 hr, pH=8, ratio of $AgNO_3$ solution to cell free extract is 2:1. Biosynthesized AgNPs were spherical with average size of 13.95nm and hydrodynamic radius average of 58.22(d. nm). The biosynthesized AgNPs were negatively charged with a charge equal to −9.85 mV as determined by zeta potential analyzer. The presence of silver metal in obtained AgNPs was confirmed using EDX and functional groups present in the fungal cell-free filtrate that may be responsible for reducing Ag ions and keeping the NPs stable FTIR estimated. Finally, the antimicrobial activity of biosynthesized AgNPs were tested and showed promising results. Also, future studies on the effect of combinations of AgNPs with known antibiotics should be considered to increase the benefit of applying both agents together. To our awareness, this is the first study on optimization of biosynthesis AgNPs by *T. stipitatus* fungus using CCD as one of response surface method.

Acknowledgement

Our sincere appreciation and gratitude to every member of the Department of Botany and Microbiology at the Faculty of Science, Damietta University, and special thanks to Mohamed M. El-Zahed for his support in this research.

Reference

Ahumada M., Suuronen E.J., Alarcon E.I. (2019) Biomolecule Silver Nanoparticle-Based Materials for Biomedical Applications. In: Martínez L., Kharissova O., Kharisov B. (eds) **Handbook of Ecomaterials**. Springer, Cham. https://doi.org/10.1007/978-3-319-68255-6_161

Asha, A. B., & Narain, R. (2020). Nanomaterials properties. In: R. Narain, **Polymer Science and Nanotechnology** (pp. 343-359). Elsevier. doi:https://doi.org/10.1016/B978-0-12-816806-6.00015-7

Baker, S., Mohan Kumar, K., Santosh, P., Rakshith, D., & Satish, S. (2015). Extracellular synthesis of silver nanoparticles by novel *Pseudomonas veronii* AS41G inhabiting Annona squamosa L. and their bactericidal activity. *Spectrochim. Acta A Mol. Biomol. Spectrosc.*, **136**, 1434–1440. https://doi.org/10.1016/j.saa.2014.10.033

Baş, D., & Boyacı, İ. H. (2007). Modeling and optimization I: Usability of response surface methodology. *J Food Eng.*, ***78*(3)**, 836–845. https://doi.org/10.1016/j.jfoodeng.2005.11.024

Basavegowda, N., & Lee, Y. R. (2014). Synthesis of Gold and Silver Nanoparticles Using Leaf Extract of *Perilla Frutescens* - A Biogenic Approach. *J Nanosci Nanotechnol.*, ***14*(6)**, 4377–4382. https://doi.org/10.1166/jnn.2014.8646

Bhatnagar, S., Kobori, T., Ganesh, D., Ogawa, K., & Aoyagi, H. (2019). Biosynthesis of Silver Nanoparticles Mediated by Extracellular Pigment from *Talaromyces purpurogenus* and Their Biomedical Applications. *Nanomaterials*, ***9*(7)**, 1042. https://doi.org/10.3390/nano9071042

Bhushan, B. (2017). **Springer Handbook of Nanotechnology**. Springer Berlin Heidelberg. https://doi.org/10.1007/978-3-662-54357-3

Collera-Zúñiga, O., García Jiménez, F., & Meléndez Gordillo, R. (2005). Comparative study of carotenoid composition in three mexican varieties of *Capsicum annuum L. Food Chem.*, ***90*(1–2)**, 109–114. https://doi.org/10.1016/j.foodchem.2004.03.032

Dada, A. O., Adekola, F. A., Adeyemi, O. S., Bello, O. M., Oluwaseun, A. C., Awakan, O. J., & Grace, F.-A. A. (2018). Exploring the Effect of Operational Factors and Characterization Imperative to the Synthesis of Silver Nanoparticles. In: *Silver Nanoparticles - Fabrication, Characterization and Applications*. InTech. https://doi.org/10.5772/intechopen.76947

El-Naggar, N. E.-A., Abdelwahed, N. A. M., & Darwesh, O. M. M. (2014). Fabrication of Biogenic Antimicrobial Silver Nanoparticles by *Streptomyces aegyptia* {NEAE} 102 as Eco-Friendly Nanofactory. *J Microbiol Biotechnol.*, ***24*(4)**, 453–464. https://doi.org/10.4014/jmb.1310.10095

El-Zahed, M. M., Baka, Z., Abou-Dobara, M. I., & El-Sayed, A. (2021). In Vitro Biosynthesis and Antimicrobial Potential of Biologically Reduced Graphene Oxide/Ag Nanocomposite at Room Temperature. *J microbiol biotechnol food sci.*, ***10*(6)**, e3956–e3956.

Femi-Adepoju, A. G., Dada, A. O., Otun, K. O., Adepoju, A. O., & Fatoba, O. P. (2019). Green synthesis of silver nanoparticles using terrestrial fern (*Gleichenia pectinata* (Willd.) C. Presl.): characterization and antimicrobial studies. *Heliyon*, ***5*(4)**, e01543. https://doi.org/10.1016/j.heliyon.2019.e01543

Guo, X., Zhang, Q., Ding, X., Shen, Q., Wu, C., Zhang, L., & Yang, H. (2016). Synthesis and application of several sol–gel-derived materials via sol–gel process combining with other technologies: a review. *J Sol-Gel Sci Technol.,* ***79*(2)**, 328–358. https://doi.org/10.1007/s10971-015-3935-6

Hamedi, S., Ghaseminezhad, M., Shokrollahzadeh, S., & Shojaosadati, S. A. (2017). Controlled biosynthesis of silver nanoparticles using nitrate reductase enzyme induction of filamentous fungus and their antibacterial evaluation. *Artif Cells Nanomed Biotechnol.*, ***45*(8)**, 1588–1596. https://doi.org/10.1080/21691401.2016.1267011

Jagadeesh, B. H., Prabha, T. N., & Srinivasan, K. (2004). Activities of β-hexosaminidase and α-mannosidase during development and ripening of bell capsicum (*Capsicum annuum* var. variata). *Plant Sci.*, **167(6)**, 1263–1271. https://doi.org/10.1016/j.plantsci.2004.06.031

Kate, S., Sahasrabudhe, M., & Pethe, A. (2020). Biogenic Silver Nanoparticle Synthesis, Characterization and its Antibacterial activity against Leather Deteriorates. *Jordan J Biol Sci.*, ***13*(4)**, 493–498.

Majeed, M. I., Bhatti, H. N., Nawaz, H., & Kashif, M. (2019). Nanobiotechnology: Applications of Nanomaterials in Biological Research. In: Shahid ul-Islam (Ed.), **Integrating Green Chemistry and Sustainable Engineering** (pp. 581–615). John Wiley & Sons, Inc. https://doi.org/10.1002/9781119509868.ch17

Nour El-Dein, M. M., Baka, Z. A. M., Abou-Dobara, M. I., El-Sayed, A. K., & El-Zahed, M. M. (2021). Extracellular Biosynthesis, Optimization, Characterization and Antimicrobial Potential of *Escherichia Coli* D8 Silver Nanoparticles. *J microbiol biotechnol food sci.*, ***10*(4)**, 648–656.

Owaid, M. N., Naeem, G. A., Muslim, R. F., & Oleiwi, R. S. (2018). Synthesis, Characterization and Antitumor Efficacy of Silver Nanoparticle from *Agaricus bisporus* Pileus, Basidiomycota. *Walailak J Sci & Tech. (WJST)*, ***17*(2)**, 75–87. https://doi.org/10.48048/wjst.2020.5840

Phanjom, P., & Ahmed, G. (2017). Effect of different physicochemical conditions on the synthesis of silver nanoparticles using fungal cell filtrate of *Aspergillus oryzae* ({MTCC} No. 1846) and their antibacterial effect. *Adv Nat Sci: Nanosci Nanotechnol.*, ***8*(4)**, 45016. https://doi.org/10.1088/2043-6254/aa92bc

Raja, S., Ramesh, V., & Thivaharan, V. (2017). Green biosynthesis of silver nanoparticles using *Calliandra haematocephala* leaf extract, their antibacterial activity and hydrogen peroxide sensing capability. *Arab J Chem.*, ***10*(2)**, 253–261. https://doi.org/10.1016/j.arabjc.2015.06.023

Rose, G. K., Soni, R., Rishi, P., & Soni, S. K. (2019). Optimization of the biological synthesis of silver nanoparticles using *Penicillium oxalicum* GRS-1 and their antimicrobial effects against common food-borne pathogens. *Green Processing and Synthesis*, ***8*(1)**, 144–156. https://doi.org/10.1515/gps-2018-0042

Saifuddin, N., Wong, C. W., & Yasumira, A. A. N. (2009). Rapid Biosynthesis of Silver Nanoparticles Using Culture Supernatant of Bacteria with Microwave Irradiation. *J Chem.*, ***6*(1)**, 61–70. https://doi.org/10.1155/2009/734264

Sharma, G., Nam, J.-S., Sharma, A., & Lee, S.-S. (2018). Antimicrobial Potential of Silver Nanoparticles Synthesized Using Medicinal Herb *Coptidis rhizome*. *Molecules*, ***23*(9)**, 2268. https://doi.org/10.3390/molecules23092268

Siddiqui, M. H., Al-Whaibi, M. H., Firoz, M., & Al-Khaishany, M. Y. (2015). Role of Nanoparticles in Plants. In: **Nanotechnology and Plant Sciences** (pp. 19–35). Springer International Publishing. https://doi.org/10.1007/978-3-319-14502-0_2

Vega-Baudrit, J., Gamboa, S. M., Rojas, E. R., & Martinez, V. V. (2019). Synthesis and characterization of silver nanoparticles and their application as an antibacterial agent. *Int J Biosens Bioelectron.*, **5(5)**. https://doi.org/10.15406/ijbsbe.2019.05.00172

White, T. J., Bruns, T., Lee, S., and Taylor, J. (1990). Amplification and direct sequencing of fungal ribosomal RNA genes for phylogenetics, In: M. A. Innis, D. H. Gelfand, J. J. Sninsky, and T. J. White (Eds.), **PCR Protocols: A Guide to Methods and Applications**, (New York, NY: Academic Press), 315–322. doi: 10.1016/b978-0-12-372180-8.50042-1

Yakovlev, A. V, & Golubeva, O. Y. (2014). Synthesis Optimisation of Lysozyme Monolayer-Coated Silver Nanoparticles in Aqueous Solution. *J Nanomaterials*, ***2014***, 1–8. https://doi.org/10.1155/2014/460605

Zhang, X.-F., Liu, Z.-G., Shen, W., & Gurunathan, S. (2016). Silver Nanoparticles: Synthesis, Characterization, Properties, Applications, and Therapeutic Approaches. *Int J Mol Sci*.**, *17*(9)**, 1534. https://doi.org/10.3390/ijms17091534.